Magnetization process of the breathing pyrochlore magnet $CuInCr_4S_8$ in ultrahigh magnetic fields up to 150 T

Masaki Gen,[1,*] Yoshihiko Okamoto,[2] Masaki Mori,[2] Koshi Takenaka,[2] and Yoshimitsu Kohama[1,†]
[1]*Institute for Solid State Physics, University of Tokyo, Kashiwa, Chiba 277-8581, Japan*
[2]*Department of Applied Physics, Nagoya University, Nagoya 464-8603, Japan*

(Received 4 October 2019; revised manuscript received 7 January 2020; accepted 6 February 2020; published 24 February 2020)

The magnetization process of the breathing pyrochlore magnet $CuInCr_4S_8$ has been investigated in ultrahigh magnetic fields up to 150 T. Successive phase transitions characterized by a substantially wide 1/2-plateau from 65 T to 112 T are observed in this system, resembling those reported in chromium spinel oxides. In addition to the 1/2-plateau phase, the magnetization is found to exhibit two inherent behaviors: A slight change in the slope of the M-H curve at ∼85 T and a shoulderlike shape at ∼135 T prior to the saturation. Both of them are accompanied by a hysteresis, suggesting first-order transitions. The theoretical calculation applicable to $CuInCr_4S_8$ is also shown, based on the microscopic model with the spin-lattice coupling. The calculation fairly well reproduces the main features of the experimentally observed magnetization process, including a relatively wide cant 2:1:1 phase clearly observed in the previous work [Y. Okamoto *et al.*, J. Phys. Soc. Jpn. **87**, 034709 (2018)]. The robust 1/2-plateau on $CuInCr_4S_8$ seems to be originated from the dominant antiferromagnetic exchange interactions and the strong spin-lattice coupling.

DOI: 10.1103/PhysRevB.101.054434

I. INTRODUCTION

Frustrated spin systems have been extensively studied for several decades because they can exhibit macroscopically degenerate ground states such as quantum spin liquid [1,2]. In real compounds, however, the macroscopic degeneracy is lifted by various perturbations such as quantum and thermal fluctuations [2], spin-lattice coupling [3], Dzyaloshinskii-Moriya interaction [4], and so on. Intriguingly, such perturbations can induce successive phase transitions under magnetic fields, including unconventional magnetic phases as represented by a magnetization plateau.

Chromium spinel oxides ACr_2O_4 (A = Hg, Cd, Zn, and Mg) are well known as typical 3D frustrated magnets exhibiting field-induced successive phase transitions [5–13]. In these systems, nonmagnetic divalent cations occupying the tetrahedral A sites form a diamond lattice, whereas magnetic Cr^{3+} ions octahedrally surrounded by oxygen ions form a pyrochlore lattice. The orbital degrees of freedom are quenched because of the half-filled t_{2g} orbitals, making Cr spinel oxides an ideal $S = 3/2$ Heisenberg spin system with strong geometrical frustration. This frustration suppresses the antiferromagnetic (AFM) long-range ordering well below the Weiss temperature, i.e., $T_N \ll |\Theta_{CW}|$ [5,14–17]. The strength of the nearest-neighbor (NN) exchange interaction strongly depends on the Cr-Cr distance [18,19], indicative of a strong spin-lattice coupling, and consequently, the frustration is resolved due to the spin Jahn-Teller effect at T_N [20,21]. The spin-lattice coupling is also responsible for the robust 1/2-plateau phase with a 3-up 1-down spin configuration that appears universally in these oxide compounds [5–13,22–26]. Recently, A-site ordered Cr spinel oxides $LiMCr_4O_8$ (M = In, Ga) have attracted attention [27–34]. In these systems, Cr^{3+} ions form a breathing pyrochlore lattice comprised of an alternating array of small and large tetrahedra, characterized by two kinds of NN AFM exchange interactions, J and J', respectively [28]. The difference in the strengths of J and J' might introduce unconventional magnetic properties in high magnetic fields, distinct from ACr_2O_4. $LiMCr_4O_8$ possesses extremely strong NN AFM interactions, as indicated by the large Weiss temperature ($\Theta_{CW} = -332$ K and -659 K for M = In and Ga, respectively [28]). Thus, the saturation field is anticipated to be several hundred tesla, which can be accessed only by the electromagneto flux compression (EMFC) system [11,12]. At the present, the observation up to saturation on $LiMCr_4O_8$ has not yet been achieved due to the measurement difficulty [35].

Here, we report a combined experimental and theoretical investigation into the magnetization process of an A-site ordered Cr spinel sulfide, $CuInCr_4S_8$, on which the Weiss temperature is known to be $-7(2) \times 10^1$ K [41], suggesting that the saturation field is experimentally more accessible. The fundamental magnetic properties of this compound were investigated in the 1970s [36–40] and refocused by Okamoto *et al.* recently [41]. The heat capacity of $CuInCr_4S_8$ shows a sharp peak at $T_p = 28$ K with a sudden drop in the magnetic susceptibility, suggesting the magnetic ordering below T_p [41]. The previous neutron diffraction experiment clarified that the spin structure at 4.2 K is a collinear order comprising decoupled (100) ferromagnetic (FM) planes [37,39]. This strongly indicates the coexistence of AFM J and FM J' for small and large tetrahedra, respectively. The magnetization process of $CuInCr_4S_8$ has been revealed up to 73 T, where M reaches 45% of the saturation magnetization

*gen@issp.u-tokyo.ac.jp
†ykohama@issp.u-tokyo.ac.jp

of $M_s = 3.06\,\mu_B$/Cr (this value is estimated from the Landé g factor of 2.04) [41]. The magnetization shows a jump at ∼20 T with a large hysteresis loop and exhibits a kink at ∼35 T, suggesting a first-order phase transition. Another magnetization kink appears at ∼65 T followed by a plateaulike behavior, which may be a phase transition to the 1/2-plateau phase. In this study, we performed magnetization measurements on $CuInCr_4S_8$ under ultrahigh magnetic fields up to 150 T to elucidate the full magnetization process. We also theoretically investigated the magnetization curve of the breathing pyrochlore magnet by using a microscopic model with the spin-lattice coupling. Achievement of these works can help us understand the high-field properties of a novel type of the pyrochlore spin system that consists of two kinds of NN exchange interactions with opposite sign.

This paper is organized as follows. In Sec. II, we show the experimental method and the result of high-field magnetization measurements. The details of measurement technique are described in Supplemental Material [42]. In Sec. III, we introduce the microscopic Heisenberg model incorporating the spin-lattice coupling, which can be applied to the breathing pyrochlore magnet with $J > 0$ and $J' < 0$. The numerical calculation on the effective spin model gives a detailed and general phase diagram and magnetization curves for $CuInCr_4S_8$. In Sec. IV, we compare the calculated magnetization curves with the experimentally observed ones and discuss the characteristic features for $CuInCr_4S_8$. Finally, the possible spin structures on $CuInCr_4S_8$ under magnetic fields are proposed, and the strengths of several exchange interactions on $CuInCr_4S_8$ are also estimated.

II. EXPERIMENT

A polycrystalline powder sample of $CuInCr_4S_8$, synthesized by a solid-state reaction method as in Ref. [41], was used in the present work. The lattice parameter was found to be $a = 10.05970(11)$ Å, and the amount of intersite defects was estimated at most 3%. High-field magnetization measurements were performed using a horizontal single-turn-coil (HSTC) system up to 150 T. The pulsed-field duration time was approximately 7.3 μs. The induction method was adopted to detect the dM/dt signal using a coaxial-type self-compensated magnetization pickup coil. In order to minimize the uncompensated contribution of the background signal, three sets of measurements, in the order of sample-out, sample-in, and sample-out, were carried out as in Ref. [34]. The detailed procedure to obtain high-quality magnetization data under magnetic fields up to 150 T is described in Supplemental Material [42]. The magnetic field was measured by a calibrated pickup coil wound around the magnetization pickup coil. The sample was cooled down to approximately 5 K using a liquid-He flow cryostat made of glass epoxy (G-10). The temperature was monitored by a RuO_2 resistance thermometer.

The M-H curves (up to 134 T and 150 T) and the derivative dM/dH (up to 150 T) of $CuInCr_4S_8$ are shown in Fig. 1. The absolute magnetization values are calibrated by comparing the M-H curves with the previous magnetization data up to 73 T obtained by a nondestructive pulsed magnet [41], which is also shown in Fig. 1. Although the present data taken in HSTC have poor signal-to-noise ratio up to ∼60 T for up sweep, two sets of our data overlap quantitatively in the high-field region up to 134 T, guaranteeing the high accuracy of our measurements [42]. As seen in Fig. 1, the hysteresis opening at $\mu_0 H_{c1} \approx 17$ T (H_{c1} for down sweep) once closes in the field region from $\mu_0 H_{c2} \approx 65$ T to $\mu_0 H_{c2'} \approx 82$ T ($H_{c2'}$ for down sweep), where M is almost constant at $\sim M_s/2$, implying the 1/2-plateau phase. For both up and down sweeps, this plateaulike feature survives until $\mu_0 H_{c3} \approx 112$ T, then M clearly exhibits an upturn behavior. Note that a substantial hysteretic behavior is seen in the middle of the plateau region:

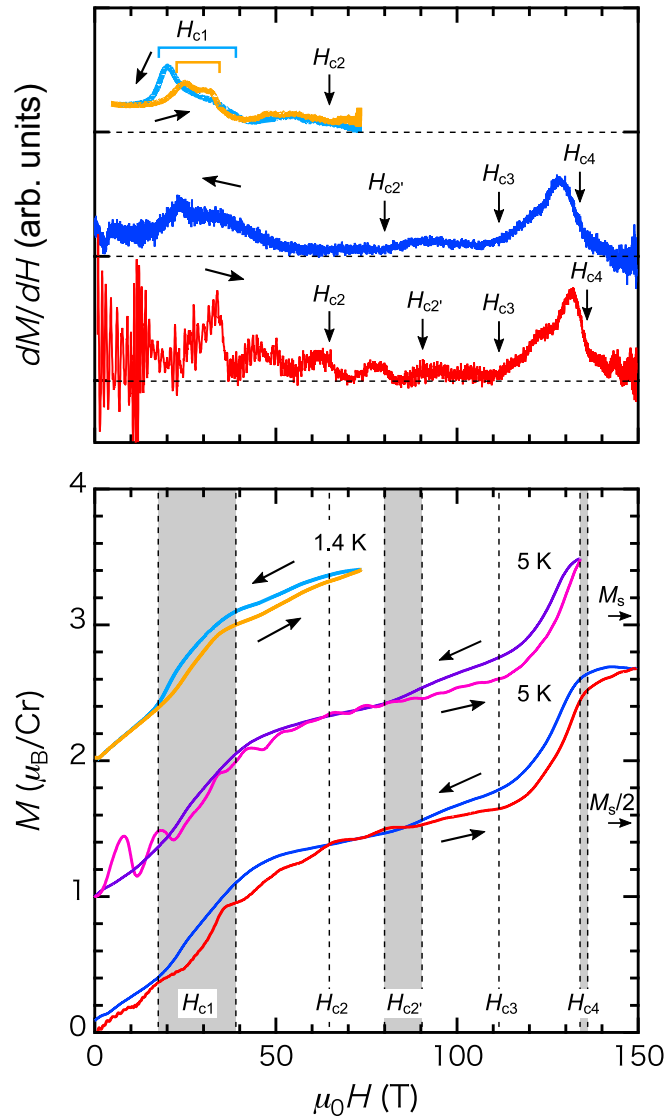

FIG. 1. M-H curves of a powder sample of $CuInCr_4S_8$ measured at approximately 5 K in a HSTC megagauss generator. Measurements were performed up to 134 T (pink and purple curves for up and down sweeps, respectively) and 150 T (red and blue curves for up and down sweeps, respectively). Derivatives dM/dH of the M-H curves up to 150 T are shown in the upper panel. The previously reported M-H curve and its derivative dM/dH measured at 1.4 K in a nondestructive pulsed magnet up to 73 T are also shown (orange and cyan curves for up and down sweeps, respectively) [41]. Each data is shifted vertically for clarity. The dashed lines in the upper panel indicate $dM/dH = 0$ lines. Transition fields are denoted by brackets or arrows in the upper panel, and drawn by the shaded areas (first order) or dashed lines (second order) in the lower panel.

TABLE I. Transition fields for $CuInCr_4S_8$ determined from the magnetization measurements under high magnetic fields. The unit is tesla.

	H_{c1}	H_{c2}	$H_{c2'}$	H_{c3}	H_{c4}	H_{sat}
up	29 ± 6	65 ± 4	90 ± 4	112 ± 2	136 ± 2	∼180
down	28 ± 11	65 ± 4	82 ± 4	112 ± 2	134 ± 2	∼180
order	1st	2nd	1st	2nd	1st	

A gradual dM/dH change is seen at ∼90 T for up sweep and at ∼82 T for down sweep. With increasing a magnetic field above the plateau phase, M exhibits a shoulderlike shape at $\mu_0 H_{c4} \approx 135$ T followed by a gradual increase until 150 T, where M reaches ∼2.7 μ_B/Cr. Assuming that M increases linearly above 150 T for up sweep, the saturation field is expected to be $\mu_0 H_{sat} \approx 180$ T. Judging from the fact that M reaches the value of $M_s/2$ at ∼90 T for up sweep, this estimation could be plausible.

The transition fields for $CuInCr_4S_8$ are summarized in Table I. There are in total six phase transitions up to the full saturation, resulting in a complicated magnetization process. $H_{c1} \sim H_{c4}$ are determined from the change in the slope of the M-H curve, although the corresponding anomalies are also visible in dM/dH as indicated by brackets or arrows in the upper panel of Fig. 1. Here, we deduce H_{c1} and H_{c2} from the previous magnetization data in Ref. [41] and take the value of H_{c1} with a large error of approximately ±10 T because the broad metamagnetic behavior is seen in dM/dH for both up and down sweeps. Note that our magnetization data did not show a clear anomaly around H_{c2} in dM/dH for down sweep, unlike that observed in a nondestructive pulsed magnet [41]. This might be the influence of the fast field-sweep rate or the magnetic-field inhomogeneity in the STC method, which becomes inevitable for down sweep due to the deformation of the field generation coil. We attribute the transitions at H_{c1}, $H_{c2'}$, and H_{c4} to the first order due to the existence of a hysteresis in the M-H curve and ones at H_{c2} and H_{c3} to the second order. For H_{c4}, the hysteretic behavior is more obviously seen in dM/dH. The detailed explanations on the experimental result are given in the following sections in combination with the theoretical analysis.

III. CALCULATION

As mentioned above, chromium spinel oxides ACr_2O_4 exhibit a variety of field-induced magnetic phases, represented by a robust 1/2-plateau phase. Although several theoretical studies have been devoted to the Cr spinel oxides [22–26,43], the ground state of the breathing pyrochlore under magnetic fields has not been investigated so far. For the sake of the interpretation of the observed magnetization process, we constructed an effective spin model on the breathing pyrochlore magnet with $J > 0$ and $J' < 0$ and examined the ground state under magnetic fields.

A. Bond-phonon model and site-phonon model

First, we introduce two microscopic models considering the spin-lattice coupling used for a standard pyrochlore antiferromagnet. One was first proposed by Penc *et al.* [22], called the bond-phonon (BP) model, which assumes independent changes in the distance between neighboring spins, $\mathbf{S}_i$ and $\mathbf{S}_j$. In the following, we treat spins in the classical limit, and normalize to $|\mathbf{S}| = 1$. The effective Heisenberg Hamiltonian of the BP model is expressed as

$$\mathcal{H}_{BP} = J \sum_{\langle i,j \rangle} [\mathbf{S}_i \cdot \mathbf{S}_j - b(\mathbf{S}_i \cdot \mathbf{S}_j)^2] - \mathbf{h} \sum_i \mathbf{S}_i, \quad (1)$$

where the summation $\langle i, j \rangle$ is taken over all the NN bonds, $\mathbf{h}$ is the magnetic field normalized by $\mathbf{h} = g\mu_B \mu_0 \mathbf{H}$, the coefficient b of the biquadratic term is a dimensionless parameter representing the strength of the spin-lattice coupling

$$b = \frac{1}{cJ} \left[\left. \frac{dJ}{dr} \right|_{r=|\mathbf{r}_{ij}^0|} \right]^2, \quad (2)$$

where c is an elastic constant, $|\mathbf{r}_{ij}|^0$ is the bond length between NN sites at their regular positions. When we take $J > 0$ and $dJ/dr < 0$, b becomes a positive value. In applied magnetic fields, the BP model can determine the local spin structure on each tetrahedron. As magnetic field is increased, the model undergoes successive phase transitions from an AFM phase to cant 2:2, 1/2-plateau, cant 3:1, then spin-saturated phases. In a weak spin-lattice coupling regime ($b \lesssim 0.05$), a cant 2:1:1 phase appears between cant 2:2 and the 1/2-plateau phases. The mechanism for stabilizing the 1/2-plateau phase can be attributed to the biquadratic term favoring a collinear spin configuration. The zero-temperature b-h phase diagram on Eq. (1) has been well understood [22,25,26], and the corresponding magnetization curves are compatible to the experimentally observed magnetization processes of ACr_2O_4 ($b = 0.15, 0.10$, and 0.02 for A = Hg, Cd, and Zn, respectively). However, the biquadratic term cannot completely reproduce the degeneracy lifting in the pyrochlore system because spin correlations beyond NN sites via the lattice distortion are not taken into account on the BP model, resulting in the absence of the magnetic long-range order [26]. This is not the case in real compounds.

Alternatively, Bergman *et al.* [24] proposed another microscopic spin model, called the site-phonon (SP) model, which assumes independent displacement of each site position. The effective Hamiltonian of the SP model is expressed as

$$\begin{aligned} \mathcal{H}_{SP} = {} & J \sum_{\langle i,j \rangle} [\mathbf{S}_i \cdot \mathbf{S}_j - b(\mathbf{S}_i \cdot \mathbf{S}_j)^2] \\ & - J \frac{b}{2} \sum_{j \neq k \in N(i)} \mathbf{e}_{ij} \cdot \mathbf{e}_{ik} (\mathbf{S}_i \cdot \mathbf{S}_j)(\mathbf{S}_i \cdot \mathbf{S}_k) \\ & - \mathbf{h} \sum_i \mathbf{S}_i, \end{aligned} \quad (3)$$

where $\mathbf{e}_{ij}$ denotes the unit vector connecting NN sites i and j at their regular positions, $N(i)$ denotes the set of NN sites of site i. In addition to the biquadratic term as present in the BP model, the SP model includes an additional three-body term derived from the effective second- and third-NN interactions caused by the lattice distortion. Since the biquadratic term still plays a dominant role on the SP model, the basic feature of the magnetization curve remains unchanged. On the other hand, the additional term in Eq. (3) reduces the macroscopic degeneracy of the spin degrees of freedom, leading to the magnetic long-range order. For example, in the zero-field

ordered state, a tetragonal collinear spin structure with (1,1,0) magnetic Bragg peaks is predicted for $b < 0.25$ [44]. This is consistent with the neutron scattering experiments on ACr_2O_4 where the observed Bragg-peak patterns involve (1,1,0) reflections although they are composed of rich and complex reflections [14,45,46]. Furthermore, the SP model predicts a 16-sublattice cubic spin structure with space group $P4_332$ for the 1/2-plateau phase. This spin structure was also observed in high-field neutron scattering experiments on $HgCr_2O_4$ and $CdCr_2O_4$ [45,47].

B. Effective spin model applicable to $CuInCr_4S_8$

Here, let's move to the case of the breathing pyrochlore lattice. Recently, Aoyama *et al.* [48] derived a SP model in the presence of breathing lattice distortion. The Heisenberg Hamiltonian considering two kinds of NN exchange interactions, J and J', is written as

$$\mathcal{H}_0 = J \sum_{\langle i,j\rangle_S} \mathbf{S}_i \cdot \mathbf{S}_j + J' \sum_{\langle i,j\rangle_L} \mathbf{S}_i \cdot \mathbf{S}_j, \tag{4}$$

where the summation $\langle i,j\rangle_S$ ($\langle i,j\rangle_L$) is defined only in the small (large) tetrahedra. Assuming $J, J' > 0$ and $dJ/dr, dJ'/dr < 0$, we can define two spin-lattice coupling parameters with positive sign, b and b', in the small and large tetrahedra, respectively. Then, the spin interactions mediated by the SP effect can be expressed as

$$\begin{aligned}\mathcal{H}_{SLC} = &-Jb \sum_{\langle i,j\rangle_S} (\mathbf{S}_i \cdot \mathbf{S}_j)^2 - J'b' \sum_{\langle i,j\rangle_L} (\mathbf{S}_i \cdot \mathbf{S}_j)^2 \\ &- \sum_i \left\{ \frac{Jb}{4} \sum_{j\neq k\in N_S(i)} + \frac{J'b'}{4} \sum_{j\neq k\in N_L(i)} \right\} (\mathbf{S}_i \cdot \mathbf{S}_j)(\mathbf{S}_i \cdot \mathbf{S}_k) \\ &- \sqrt{JJ'bb'} \sum_i \sum_{j\in N_S(i)} \sum_{k\in N_L(i)} \mathbf{e}_{ij} \cdot \mathbf{e}_{ik} (\mathbf{S}_i \cdot \mathbf{S}_j)(\mathbf{S}_i \cdot \mathbf{S}_k),\end{aligned} \tag{5}$$

where $N_S(i)$ ($N_L(i)$) is defined only in the small (large) tetrahedra. The derivation process of Eq. (5) is described in Ref. [48]. As well as the case of ACr_2O_4, this Hamiltonian also stabilizes a tetragonal collinear spin structure with (1,1,0) magnetic Bragg peaks in the wide ranges of b, b', and J'/J [48], which is in agreement with the experimentally observed domain state in the low-temperature ordered phase on $LiMCr_4O_8$ (M = In, Ga) [30,31]. The investigation of b-h phase diagrams on the SP model for various values of J'/J ($0 < J'/J \leqslant 1$) is in progress [49].

Although one adopted this model to the antiferromagnet with $J, J' > 0$, it is also applicable to the case of $J > 0$ and $J' < 0$. In this process, however, we have to be careful of the preceding sign of each term in Eq. (5). In the case of $J' < 0$, the sign of dJ'/dr is nontrivial for the following reasons. In Cr spinel sulfides, the NN exchange interaction is mainly originated from the AFM direct exchange interaction between NN Cr sites and the FM superexchange interaction via Cr-S-Cr path. The difference in the Cr-Cr distance on the small and large tetrahedra is only 6% at room temperature on $CuInCr_4S_8$, so the opposite sign of J and J' implies that the AFM direct exchange and the FM superexchange interactions are competitive. Considering that the former is affected by the Cr-Cr distance whereas the latter by the Cr-S-Cr angle, which is clarified to be larger than 90° in all NN Cr pairs on $CuInCr_4S_8$ [41], the increase in the Cr-Cr distance will make both the direct exchange and the superexchange interactions weaker. Hence, both situations, $dJ'/dr < 0$ and $dJ'/dr > 0$, could be realized in $CuInCr_4S_8$. Note that the above explanation cannot remove the possibility of $dJ/dr > 0$, but the assumption of $dJ/dr < 0$ is more plausible because the direct exchange interaction becomes relatively dominant as the Cr atoms get closer. Regardless of the sign of dJ/dr and dJ'/dr, the sign of each spin-lattice coupling parameter becomes $b > 0$ and $b' < 0$ [see Eq. (2)]. However, under the assumption of $dJ/dr < 0$ and $dJ'/dr > 0$, the preceding sign of the last term in Eq. (5) changes from minus to plus [50]. In the following discussion, we will exclude this case, i.e., we will assume $dJ/dr < 0$ and $dJ'/dr < 0$ as the effect of the spin-lattice coupling. Indeed, the calculation for the case of $dJ'/dr < 0$ reproduces the experimental results better than the case of $dJ'/dr > 0$, in the sense that it reproduces the observed wide intermediate phase prior to the 1/2-plateau phase on $CuInCr_4S_8$.

In addition, we include further-neighbor (FN) AFM interactions between sites of second and third NNs, which are expected to be strong in sulfides unlike oxides [18,51]:

$$\mathcal{H}_{FN} = J_2 \sum_{\langle\langle i,j\rangle\rangle} \mathbf{S}_i \cdot \mathbf{S}_j + J_{3a} \sum_{\langle\langle\langle i,j\rangle\rangle\rangle_{3a}} \mathbf{S}_i \cdot \mathbf{S}_j + J_{3b} \sum_{\langle\langle\langle i,j\rangle\rangle\rangle_{3b}} \mathbf{S}_i \cdot \mathbf{S}_j, \tag{6}$$

where the summations $\langle\langle i,j\rangle\rangle$, $\langle\langle\langle i,j\rangle\rangle\rangle_{3a}$, and $\langle\langle\langle i,j\rangle\rangle\rangle_{3b}$ are taken for second NN and two kinds of third NN sites ($3a$ and $3b$), respectively [Fig. 2(a)]. For simplicity, we do not take care of the effects of the lattice distortion on the strengths of these FN interactions. Organizing the above, we obtain

$$\mathcal{H}_{CuInCr_4S_8} = \mathcal{H}_0 + \mathcal{H}_{SLC} + \mathcal{H}_{FN} - \mathbf{h} \sum_i \mathbf{S}_i \tag{7}$$

as the spin Hamiltonian of $CuInCr_4S_8$ under magnetic fields.

In this study, we convert this complicated model into a simple one. We naively anticipate that all four spins within the same large tetrahedron always take a ferromagnetically aligned spin configuration even in the external magnetic fields as in zero field. By treating those four spins as one localized spin at the center of a large tetrahedra, the breathing pyrochlore magnet with $J > 0$ and $J' < 0$ can be mapped onto the antiferromagnet composed of a face-centered cubic (fcc) lattice [Fig. 2(b)]. Hereafter, we will represent a spin vector $\mathbf{S}_\alpha$ as a spin located at the fcc site after the model transformation mentioned above. By omitting constant terms and assuming $Jb = J'b'$ in Eq. (7), we finally derive the effective spin Hamiltonian of $CuInCr_4S_8$ as

$$\begin{aligned}\mathcal{H}^{\text{eff}}_{CuInCr_4S_8} = &(J + 4J_2 + 2J_{3a} + 2J_{3b}) \sum_{\langle\alpha,\beta\rangle} \mathbf{S}_\alpha \cdot \mathbf{S}_\beta \\ &- Jb \sum_{\langle\alpha,\beta\rangle} (\mathbf{S}_\alpha \cdot \mathbf{S}_\beta)^2 + 4Jb \sum_{\langle\alpha,\beta\rangle} \mathbf{S}_\alpha \cdot \mathbf{S}_\beta \\ &- \frac{Jb}{4} \sum_k \sum_{\alpha\neq\beta\neq\gamma\in k} (\mathbf{S}_\alpha \cdot \mathbf{S}_\beta)(\mathbf{S}_\alpha \cdot \mathbf{S}_\gamma) \\ &- \frac{\mathbf{h}}{4} \sum_\alpha \mathbf{S}_\alpha,\end{aligned} \tag{8}$$

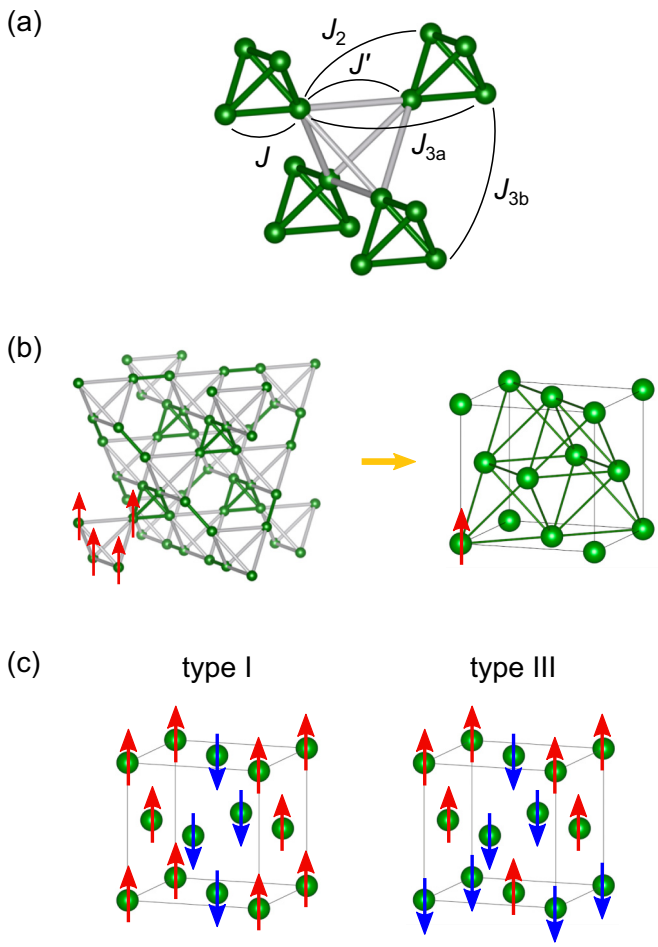

FIG. 2. (a) Crystal structure of the breathing pyrochlore lattice with two kinds of NN exchange interactions, J and J', in the small and large tetrahedra, respectively. Second NN (J_2) and third NN interactions (J_{3a} and J_{3b} for two symmetrically inequivalent paths) are also shown. (b) Model transformation from the breathing pyrochlore magnet with $J > 0$ and $J' < 0$ to the fcc lattice antiferromagnet. Four spins in each large tetrahedron are converted to one localized spin, as indicated by red arrows. (c) Two types of the AFM ordering which are candidates for the ground state on the fcc lattice antiferromagnet. Up and down spins are described by red and blue arrows, respectively.

where the first summation in the fourth term are taken for all local tetrahedra k depicted in the fcc lattice of Fig. 2(b). The second term is originated from the BP effect, and the third and fourth terms from the SP effect. Note that the fcc lattice can be regarded as the 3D network of edge-sharing tetrahedra, possessing geometrical frustration. If we consider only NN interactions on the fcc lattice, two kinds of Neel orders, Type I and Type III [Fig. 2(c)], become candidates for the ground state at zero field (Type II state can be realized in the existence of FN interactions). Such a degeneracy can be lifted by fluctuations [2,52,53], FN interactions [40], and so on. Theoretically, it has been shown that fluctuations favor Type I state with an ordering wave vector $\mathbf{q} = (1, 0, 0)$. Indeed, the observed magnetic structure of $CuInCr_4S_8$ at zero field can be mapped onto Type I state [39].

C. Calculation results

In this section, we focus on the characteristics of the zero-temperature b-h phase diagram and magnetization curves derived from Eq. (8). In our analysis, the fourth- and sixth-NN interactions in the original breathing pyrochlore lattice are not taken into account. Consequently, only NN interactions and intratetrahedral interactions appear in the effective Hamiltonian on the fcc lattice. Thus, we can rewrite Eq. (8) by taking a summation of local Hamiltonian on each single tetrahedron:

$$\mathcal{H}^{\rm eff}_{\rm CuInCr_4S_8} = \sum_k \mathcal{H}^{\rm local}_{\rm CuInCr_4S_8}, \tag{9}$$

$$\begin{aligned}\mathcal{H}^{\rm local}_{\rm CuInCr_4S_8} = {} & [J(1+4b) + J_{\rm FN}] \sum_{\langle\alpha,\beta\rangle_k} \mathbf{S}_\alpha \cdot \mathbf{S}_\beta \\ & - Jb \sum_{\langle\alpha,\beta\rangle_k} (\mathbf{S}_\alpha \cdot \mathbf{S}_\beta)^2 \\ & - \frac{Jb}{4} \sum_{\alpha\neq\beta\neq\gamma\in k} (\mathbf{S}_\alpha \cdot \mathbf{S}_\beta)(\mathbf{S}_\alpha \cdot \mathbf{S}_\gamma) \\ & - \frac{\mathbf{h}}{4} \sum_{\alpha\in k} \mathbf{S}_\alpha,\end{aligned} \tag{10}$$

where $J_{\rm FN} \equiv 4J_2 + 2J_{3a} + 2J_{3b}$, and the summation $\langle\alpha, \beta\rangle_k$ is taken over all pairs in a single tetrahedron k. Here, we normalize spin vectors to $|\mathbf{S}_\alpha| = 1$, and choose $J_{\rm FN}/J$ and b as adjustable dimensionless parameters. Since all the optimum spin configurations on each local tetrahedron can be simultaneously satisfied on the fcc lattice with an infinite size, we can obtain the ground state just by numerically minimizing Eq. (10) at arbitrary strength of the magnetic field.

The b-h phase diagram and the corresponding magnetization curves for given values of b are summarized in Fig. 3. Regardless of the value of $J_{\rm FN}/J$, the b-h phase diagram becomes identical except the scale of both axes. Here, we demonstrate the case of $J_{\rm FN}/J = 0$. As shown in Fig. 3(a), several magnetic phases such as cant 2:2, cant 2:1:1, 1/2-plateau, cant 3:1, and spin-saturated phases appear in applied magnetic fields. We define h_{c1}, h_{c2}, h_{c3}, and $h_{\rm sat}$ as transition fields to the cant 2:1:1, 1/2-plateau, cant 3:1, and spin-saturated phases, respectively. For $b \lesssim 0.17$, the cant 2:1:1 phase appears immediately below the 1/2-plateau phase. The transition from the cant 2:2 to cant 2:1:1 phase at h_{c1} is the first order accompanied by a magnetization jump. The transition from the cant 2:1:1 to 1/2-plateau phase at h_{c2} is the second order for $b \lesssim 0.12$, where the value of $h_{c2}/4$ is constant to $4J$, while it turns to the first order for $b \gtrsim 0.12$, where h_{c2} becomes slightly higher as b increases. The transition field h_{c1} gets monotonously higher as b increases, and finally merges with h_{c2} at $b \approx 0.17$. For $b \gtrsim 0.17$, a first-order transition from the cant 2:2 to 1/2-plateau phase occurs at h_{c2}, accompanied by a magnetization jump. The width of the 1/2-plateau phase is extremely broad, indicating that the 3-up 1-down spin configuration with the magnetization $M/M_s = 1/2$ is stable in a wide field region. When a higher magnetic field is applied in the 1/2-plateau phase, the system undergoes a second-order transition to the cant 3:1 phase at $h_{c3}/4 = 4(1 + 6b)J$, then finally enters the spin-saturated phase at $h_{\rm sat}$. The transition from the cant 3:1 to spin-saturated phase is the second order

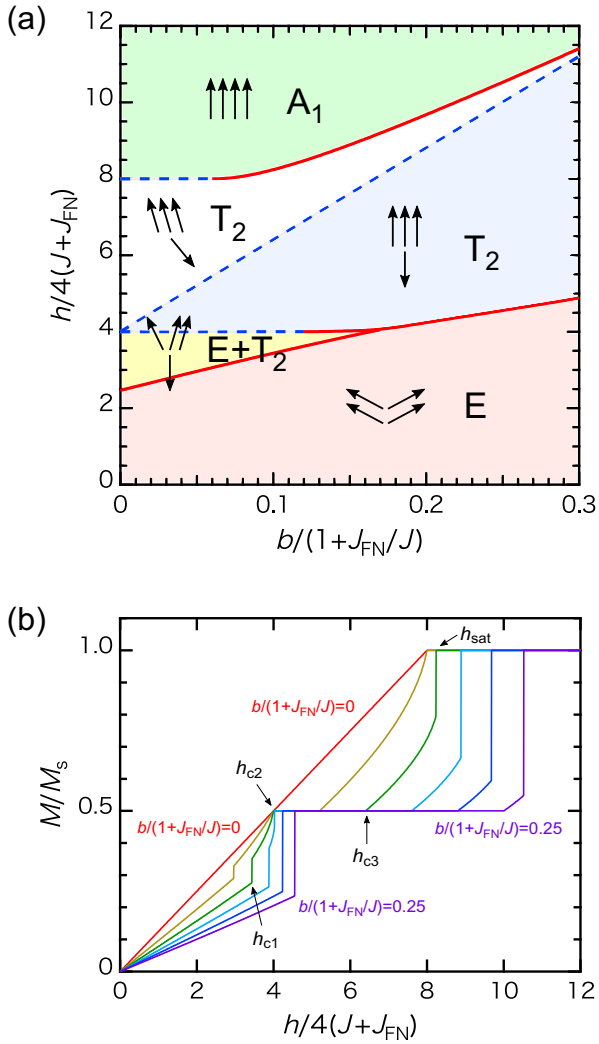

FIG. 3. (a) Phase diagram of Eq. (10) as a function of the spin-lattice coupling parameter b and magnetic field h. Red solid and blue dashed lines denote first- and second-order transitions, respectively. The regions shaded in pink, yellow, blue, white, and green express a cant 2:2, cant 2:1:1, 1/2-plateau, cant 3:1, and fully polarized phase, respectively. Schematic spin configuration within a single tetrahedron and its irreducible representation of the tetrahedral symmetry group are also illustrated in each region. This phase diagram is applicable to any value of $J_{\rm FN}$. (b) Magnetization curves as a function of magnetic field h for $b/(1+J_{\rm FN}/J) = 0$ to 0.25 in steps of 0.05. The transition fields, h_{c1}, h_{c2}, h_{c3}, and $h_{\rm sat}$, are indicated for the case of $b/(1+J_{\rm FN}/J) = 0.10$ as example.

for $b \lesssim 0.06$, where the value of $h_{\rm sat}/4$ is constant to $8J$, while it becomes the first order for $b \gtrsim 0.06$, where $h_{\rm sat}$ increases gradually as b increases.

Although the b-h phase diagram of Eq. (10) is similar with that of Eq. (1) proposed in Ref. [22], there are two remarkable differences. First, as b increases the broadening of the 1/2-plateau phase becomes saturated for Eq. (1), whereas the width of the 1/2-plateau becomes constantly wider in our model. Second, the cant 2:1:1 phase emerges in wider ranges of b and h in our results. If we adopt the BP model to the breathing pyrochlore magnet with $J > 0$ and $J' < 0$, the effective Hamiltonian becomes identical with Eq. (1). Hence, the differences in the b-h phase diagram can be attributed to the effective FN interactions caused by the local lattice distortion, which is only taken into account on the SP model [the third and fourth terms of Eq. (8)].

IV. DISCUSSION AND CONCLUSION

A few experimental studies have been made under high magnetic fields on $CuInCr_4S_8$ so far [40,41]. Despite these efforts, there is still little understanding on the field-induced magnetic phases. Here, we compare our experimental and theoretical results on $CuInCr_4S_8$ with those on Cr spinel oxides, and discuss how our research contributes to the fundamental understanding of the magnetization process of $CuInCr_4S_8$.

In the low-field region below 70 T, two phase transitions at H_{c1} and H_{c2} are observed prior to the 1/2-plateau. The former is the first-order phase transition which is accompanied by a large hysteresis and associated with a cusp in dM/dH, whereas the latter might be the second order because a broad hump structure in dM/dH between 40 T and 65 T almost overlaps for up and down sweeps as shown in the upper panel of Fig. 1 (visible only in the result obtained by a nondestructive pulsed magnet [41]). The calculated magnetization curve with a small spin-lattice coupling parameter ($b \lesssim 0.17$) shown in Fig. 3(b) well reproduces these two-step phase transitions qualitatively. Hence, the intermediate phase between H_{c1} and H_{c2} can be identified with a cant 2:1:1 phase. The cant 2:1:1 phase has already been observed for $ZnCr_2O_4$ (120 $\sim$ 135 T) [10] and $MgCr_2O_4$ (125 $\sim$ 140 T) [13] by optical Faraday rotation measurements, but its field region is rather narrow compared to the cant 2:2 phase. In contrast, the M-H curve of $CuInCr_4S_8$ seems to show a relatively broad cant 2:1:1 phase although it is difficult to define the precise values of H_{c1} and H_{c2}. Such a broad cant 2:1:1 phase is reproduced better by our theoretical calculation based on the SP model rather than the BP model [22]. After reaching the 1/2-plateau phase at H_{c2}, the magnetization slowly increases until H_{c3} then shows a substantial upturn behavior. Our theoretical calculation suggests a second-order phase transition from the 3:1 collinear spin state to the spin-canted state without any change in the lattice symmetry at h_{c3}, where the magnetization starts increasing again. Given that no hysteretic behavior is observed in dM/dH at H_{c3}, it seems plausible to ascribe H_{c3} to h_{c3}. As shown in Fig. 3(b), if the magnetization changes linearly in higher fields than h_{c1}, it will reach $M_s/2$ at around h_{c3} regardless of the value of b. On the other hand, the linear fit of the experimental M-H curve below H_{c1} will cross the $M = M_s/2$ value at $\sim$70 T, which is much lower than the value of the observed $\mu_0 H_{c3} \approx 112$ T. There are a few possible reasons for this behavior. One is that we restrict our theoretical analysis on the simple case of the equal coupling in different symmetry $b_{A_1} = b_E = b_{T_2}$. When we adopt the microscopic model to real compounds, we can assume different values of b, i.e., $b_{A_1} \neq b_E \neq b_{T_2}$ [22,25,54]. Indeed, b_{T_2} seems larger than b_E for $HgCr_2O_4$ and $CdCr_2O_4$ [54], which might also be true for $CuInCr_4S_8$. Another possible reason is that AFM FN interactions might become stronger in the 1/2-plateau phase due to the lattice distortion. In order to accurately account for the observed value of H_{c3}, it is necessary to estimate the change in the FN interactions caused by the magnetostriction.

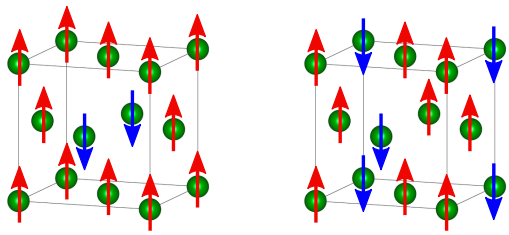

FIG. 4. Two possible 3-up 1-down spin structures for the 1/2-plateau phase on the fcc lattice. Up and down spins are described by red and blue arrows, respectively.

In addition to these phase transitions, two exotic features are observed in the M-H curve of $CuInCr_4S_8$, which cannot be explained by our theoretical calculation. (i) First, a gradual dM/dH change appears at $H_{c2'}$ accompanied by a hysteresis. Since this behavior was well reproduced by several measurements with different maximum magnetic fields, the technical issue of measurements can be excluded [42]. As mentioned above, it is natural to consider that H_{c2} and H_{c3} correspond to h_{c2} and h_{c3} defined in our calculated results, respectively. Accordingly, the magnetic structure between H_{c2} and H_{c3} should be the 3-up 1-down spin configuration, analogous to the 1/2-plateau phase realized in Cr spinel oxides. One possible mechanism for the first-order nature at $H_{c2'}$ is the change in the global spin structure accompanied by the lattice distortion while maintaining the 3-up 1-down spin configuration in small Cr_4 tetrahedra. The present theory cannot take into account such a scenario because our microscopic spin model focuses only on the local spin structure of four sites in the mapped fcc lattice, i.e., the spin structure of 16 sites in the original breathing pyrochlore lattice. Importantly, two kinds of global spin structure are possible for the 1/2-plateau phase in our model, as shown in Fig. 4. In order to lift this degeneracy, it is required to include more perturbations to calculation, which is out of the scope in this work because there is still some ambiguities about the exchange interactions on $CuInCr_4S_8$. To the best of our knowledge, a phase transition within a magnetization plateau has been reported only on $MnCr_2S_4$, which is composed of two kinds of magnetic ions Mn^{2+} ($S = 5/2$) and Cr^{3+} ($S = 3/2$) occupying the tetrahedral A and octahedral B sites of the spinel structure AB_2X_4, respectively [55]. In the case of $MnCr_2S_4$, however, such a transition was hardly detected as anomalies in the M-H curve while it was clearly observed by the ultrasound measurements. It should be noted that the magnetocaloric effect cannot be ignored in our magnetization data of $CuInCr_4S_8$ because the measurement condition in the STC system is close to adiabatic due to the fast field-sweep rate. Although we speculate the hysteretic behavior at $H_{c2'}$ is mainly related to the change in the spin state, a dedicated technique sensitive to the lattice deformation under high magnetic fields might be required to understand such an exotic feature in the M-H curve. (ii) Second, the M-H curve of $CuInCr_4S_8$ exhibits a shoulderlike behavior characterized by a sharp peak in dM/dH around H_{c4}, where M reaches $\sim 2.5\,\mu_B$/Cr, which is much smaller than $M_s = 3.06\,\mu_B$/Cr. It suggests the existence of another intermediate phase between cant 3:1 and spin-saturated phases. In the series of Cr spinel oxides ACr_2O_4 (A = Hg, Cd, and Zn), a shoulderlike behavior in the M-H curve and a drastic change in the intensity of the optical absorption associated with an exciton-magnon-phonon process have been reported just before the full saturation of magnetization [7,9,11]. In the case of $HgCr_2O_4$, a first-order structural transformation to the crystal structure with A_1 symmetry was predicted at this phase transition by the previous ESR study [6]. This intermediate phase is now believed to be a spin-nematic phase after the theoretical proposal incorporating the quantum effect [43]. Recently, the ground state of the $S = 1/2$ Heisenberg model on the fcc lattice under magnetic fields was also investigated by Morita *et al.* [56]. The magnetization curve on the $S = 1/2$ fcc lattice without tetragonal distortion is quite similar with our results [Fig. 3(b)], exhibiting cant 2:2, cant 2:1:1, 1/2-plateau, cant 3:1, and spin-saturated phases. In this case, the tetragonal distortion on the fcc lattice induces more diverse supersolid phases immediately below the 1/2-plateau and the spin-saturated phase. This distortion can be regarded as the lattice distortion caused by the spin-lattice coupling on the isotropic fcc lattice. Thus, these quantum phases might also be relevant to our experimental observation although $CuInCr_4S_8$ is a $S = 3/2$ system.

Finally, we remark on the estimation of the exchange interactions on $CuInCr_4S_8$. Under the mean-field approximation, the Weiss temperature Θ_{CW} and the saturation field H_{sat} can be deduced as follows, respectively:

$$\Theta_{CW} = -\frac{S(S+1)}{k_B}(J + J' + J_{FN}), \tag{11}$$

$$\mu_0 H_{sat} = \frac{8S}{g\mu_B}(J + J_{FN}), \tag{12}$$

where k_B is the Boltzmann's constant. By combining two formulas Eqs. (11) and (12), $J + J_{FN}$ and J' can be obtained independently. Previously, Plumier *et al.* [40] calculated them from the experimental results of the magnetic susceptibility and the magnetization up to 38 T by using the estimated values of $\Theta_{CW} = -77$ K and $\mu_0 H_{sat} = 146$ T, where they might mistakenly multiply a factor of 2 to the right side of Eq. (11). Here, we recalculate in the same way, which yields the exchange interactions of $(J + J_{FN})/k_B = 21$ K and $J'/k_B = -2$ K with $g = 2.04$, $\Theta_{CW} = -7 \times 10^1$ K [41], and $\mu_0 H_{sat} = 1.8 \times 10^2$ T (estimated from this study). This implies that the AFM interactions are dominant on $CuInCr_4S_8$, which could be responsible for the robust 1/2-plateau as observed in Cr spinel oxides. It should be noted that the M-H curves of $LiGaCr_4S_8$ and $LiInCr_4S_8$, where the FM interaction J' is expected to be strong, do not clearly exhibit the 1/2-plateau [41]. Recently, the exchange interactions of several Cr spinel compounds forming a breathing pyrochlore lattice were theoretically investigated by Ghosh *et al.* [51]. By using the lattice parameter of $CuInCr_4S_8$ at room temperature, the exchange interactions are obtained as $J/k_B = 14.7$ K, $J'/k_B = -26.0$ K, $J_2/k_B = 1.1$ K, $J_{3a}/k_B = 6.4$ K, and $J_{3b}/k_B = 4.5$ K. Assuming these values, the saturation field is calculated to be 3.6×10^2 T, which is much higher than the experimental observation. It seems that we have to carefully consider the influence of the spin-lattice coupling and thermal fluctuation.

To summarize, we investigated the magnetization process of the breathing pyrochlore magnet $CuInCr_4S_8$ with $J > 0$ and $J' < 0$ both experimentally and theoretically. The observed M-H curve is characterized by a wide $1/2$-plateau exhibiting from $\mu_0 H_{c2} \approx 65$ T to $\mu_0 H_{c3} \approx 112$ T, and the saturation field is estimated to be $\mu_0 H_{sat} \approx 180$ T. Two unique behaviors are also observed in the M-H curve: A slight slope change accompanied by a hysteresis at $\mu_0 H_{c2'} \approx 85$ T in the $1/2$-plateau region and a shoulderlike shape at $\mu_0 H_{c4} \approx 135$ T prior to the saturation. In particular, there are few reports on the former phenomenon, i.e., a phase transition within a magnetization-plateau state. We also proposed the microscopic classical spin model to understand the magnetic behavior of the breathing pyrochlore magnet with $J > 0$ and $J' < 0$. The calculation well reproduces the main features of the magnetization process of $CuInCr_4S_8$, especially a relatively wide cant 2:1:1 phase. However, there are still many unsolved issues in $CuInCr_4S_8$, such as the global spin structure in each phase, the possible change in the exchange interactions under magnetic fields, and so on. Further experimental investigation such as the magnetostriction, magnetocaloric effect, ultrasound, ESR, NMR, neutron, and x-ray measurements under high magnetic fields should be interesting and will provide useful clues to understand the essence of the successive phase transitions on $CuInCr_4S_8$.

ACKNOWLEDGMENTS

We appreciate for fruitful discussion to Dr. K. Morita, Dr. K. Aoyama, and Prof. H. Kawamura. This work was supported by JSPS KAKENHI Grants No. 16H03848, No. 18H01163, and No. 19H05823.

[1] P. W. Anderson, Mat. Res. Bull. **8**, 153 (1973).
[2] R. Moessner and J. T. Chalker, Phys. Rev. B **58**, 12049 (1998).
[3] O. Tchernyshyov, R. Moessner, and S. L. Sondhi, Phys. Rev. Lett. **88**, 067203 (2002).
[4] M. Elhajal, B. Canals, R. Sunyer, and C. Lacroix, Phys. Rev. B **71**, 094420 (2005).
[5] H. Ueda, H. Mitamura, T. Goto, and Y. Ueda, Phys. Rev. B **73**, 094415 (2006).
[6] S. Kimura, M. Hagiwara, T. Takeuchi, H. Yamaguchi, H. Ueda, Y. Ueda, and K. Kindo, Phys. Rev. B **83**, 214401 (2011).
[7] D. Nakamura, A. Miyata, Y. Aida, H. Ueda, and S. Takeyama, J. Phys. Soc. Jpn. **83**, 113703 (2014).
[8] E. Kojima, A. Miyata, S. Miyabe, S. Takeyama, H. Ueda, and Y. Ueda, Phys. Rev. B **77**, 212408 (2008).
[9] A. Miyata, S. Takeyama, and H. Ueda, Phys. Rev. B **87**, 214424 (2013).
[10] A. Miyata, H. Ueda, Y. Ueda, Y. Motome, N. Shannon, K. Penc, and S. Takeyama, J. Phys. Soc. Jpn. **80**, 074709 (2011).
[11] A. Miyata, H. Ueda, Y. Ueda, H. Sawabe, and S. Takeyama, Phys. Rev. Lett. **107**, 207203 (2011).
[12] A. Miyata, H. Ueda, Y. Ueda, Y. Motome, N. Shannon, K. Penc, and S. Takeyama, J. Phys. Soc. Jpn. **81**, 114701 (2012).
[13] A. Miyata, H. Ueda, and S. Takeyama, J. Phys. Soc. Jpn. **83**, 063702 (2014).
[14] J.-H. Chung, M. Matsuda, S.-H. Lee, K. Kakurai, H. Ueda, T. J. Sato, H. Takagi, K.-P. Hong, and S. Park, Phys. Rev. Lett. **95**, 247204 (2005).
[15] S.-H. Lee, C. Broholm, T. H. Kim, W. Ratcliff II, and S.-W. Cheong, Phys. Rev. Lett. **84**, 3718 (2000).
[16] S. Ji, S.-H. Lee, C. Broholm, T. Y. Koo, W. Ratcliff, and S.-W. Cheong, P. Zschack, Phys. Rev. Lett. **103**, 037201 (2009).
[17] L. Ortega-San-Martin, A. J. Williams, C. D. Gordon, S. Klemme, and J. P. Attfield, J. Phys.: Condens. Matter **20**, 104238 (2008).
[18] A. N. Yaresko, Phys. Rev. B **77**, 115106 (2008).
[19] H. Ueda and Y. Ueda, Phys. Rev. B **77**, 224411 (2008).
[20] Y. Tanaka, Y. Narumi, N. Terada, K. Katsumata, H. Ueda, U. Staub, K. Kindo, T. Fukui, T. Yamamoto, R. Kammuri, M. Hagiwara, A. Kikkawa, Y. Ueda, H. Toyokawa, T. Ishikawa, and H. Kitamura, J. Phys. Soc. Jpn. **76**, 043708 (2007).
[21] S.-H. Lee, G. Gasparovic, C. Broholm, M. Matsuda, J.-H. Chung, Y. J. Kim, H. Ueda, G. Xu, P. Zschack, K. Kakurai, H. Takagi, W. Ratcliff, T. H. Kim, and S.-W. Cheong, J. Phys.: Condens. Matter **19**, 145259 (2007).
[22] K. Penc, N. Shannon, and H. Shiba, Phys. Rev. Lett. **93**, 197203 (2004).
[23] Y. Motome, K. Penc, and N. Shannon, J. Magn. Magn. Mater. **300**, 57 (2006).
[24] D. L. Bergman, R. Shindou, G. A. Fiete, and L. Balents, Phys. Rev. B **74**, 134409 (2006).
[25] K. Penc, N. Shannon, Y. Motome, and H. Shiba, J. Phys.: Condens. Matter **19**, 145267 (2007).
[26] N. Shannon, K. Penc, and Y. Motome, Phys. Rev. B **81**, 184409 (2010).
[27] J.-C. Joubert and A. Durif, Bull. Soc. Fr. Mineral. Cristallogr. **89**, 26 (1966).
[28] Y. Okamoto, G. J. Nilsen, J. P. Attfield, and Z. Hiroi, Phys. Rev. Lett. **110**, 097203 (2013).
[29] Y. Tanaka, M. Yoshida, M. Takigawa, Y. Okamoto, and Z. Hiroi, Phys. Rev. Lett. **113**, 227204 (2014).
[30] G. J. Nilsen, Y. Okamoto, T. Masuda, J. Rodriguez-Carvajal, H. Mutka, T. Hansen, and Z. Hiroi, Phys. Rev. B **91**, 174435 (2015).
[31] R. Saha, F. Fauth, M. Avdeev, P. Kayser, B. J. Kennedy, and A. Sundaresan, Phys. Rev. B **94**, 064420 (2016).
[32] S. Lee, S.-H. Do, W.-J. Lee, Y. S. Choi, M. Lee, E. S. Choi, A. P. Reyes, P. L. Kuhns, and A. Ozarowski, K.-Y. Choi, Phys. Rev. B **93**, 174402 (2016).
[33] Y. Okamoto, D. Nakamura, A. Miyake, S. Takeyama, M. Tokunaga, A. Matsuo, K. Kindo, and Z. Hiroi, Phys. Rev. B **95**, 134438 (2017).
[34] M. Gen, D. Nakamura, Y. Okamoto, and S. Takeyama, J. Magn. Magn. Mater. **473**, 387 (2019).
[35] The magnetization measurements on $LiMCr_4O_8$ (M = In, Ga) in ultrahigh magnetic fields are on going by our group. The results will be submitted in another paper.
[36] H. L. Pinch, M. J. Woods, and E. Lopatin, Mater. Res. Bull. **5**, 425 (1970).
[37] R. Plumier, F. K. Lotgering, and R. P. van Stapele, J. Phys. Colloques **32 (C1)**, 324 (1971).

[38] W. K. Unger, H. Göbel, L. Treitinger, and H. Pink, Physica B (Amsterdam) **80**, 62 (1975).
[39] R. Plumier, M. Sougi, and M. Lecomte, Phys. Lett. A **60**, 341 (1977).
[40] R. Plumier, M. Sougi, M. Lecomte, and A. Miedan-Gros, Z. Phys. B **40**, 227 (1980).
[41] Y. Okamoto, M. Mori, N. Katayama, A. Miyake, M. Tokunaga, A. Matsuo, K. Kindo, and K. Takenaka, J. Phys. Soc. Jpn. **87**, 034709 (2018).
[42] See Supplemental Material at http://link.aps.org/supplemental/10.1103/PhysRevB.101.054434 for experimental details.
[43] E. Takata, T. Momoi, and M. Oshikawa, arXiv:1510.02373.
[44] K. Aoyama and H. Kawamura, Phys. Rev. Lett. **116**, 257201 (2016).
[45] M. Matsuda, H. Ueda, A. Kikkawa, Y. Tanaka, K. Katsumata, Y. Narumi, T. Inami, Y. Ueda, and S.-H. Lee, Nat. Phys. **3**, 397 (2007).
[46] S.-H. Lee, W. Ratcliff, Q. Huang, T. H. Kim, and S. W. Cheong, Phys. Rev. B **77**, 014405 (2008).
[47] M. Matsuda, K. Ohoyama, S. Yoshii, H. Nojiri, P. Frings, F. Duc, B. Vignolle, G. L. J. A. Rikken, L.-P. Regnault, S.-H. Lee, H. Ueda, and Y. Ueda, Phys. Rev. Lett. **104**, 047201 (2010).
[48] K. Aoyama and H. Kawamura, Phys. Rev. B **99**, 144406 (2019).
[49] K. Aoyama, M. Gen *et al.* (unpublished).
[50] This is because the preceding sign of the second term of $\mathbf{u}_i^*$ in Eq. (4) proposed in Ref. [48] is changed from plus to minus in the case of $dJ'/dr > 0$.
[51] P. Ghosh, Y. Iqbal, T. Müller, R. Thomale, J. Reuther, M. J. P. Gingras, and H. O. Jeschke, npj Quantum Mater. **4**, 63 (2019).
[52] C. L. Henley, J. Appl. Phys. **61**, 3962 (1987).
[53] O. Benton and N. Shannon, J. Phys. Soc. Jpn. **84**, 104710 (2015).
[54] S. Kimura, Y. Sawada, Y. Narumi, K. Watanabe, M. Hagiwara, K. Kindo, and H. Ueda, Phys. Rev. B **92**, 144410 (2015).
[55] V. Tsurkan, S. Zherlitsyn, L. Prodan, V. Felea, P. T. Cong, Y. Skourski, Z. Wang, J. Deisenhofer, H.-A. K. von Nidda, J. Wosnitza, and A. Loidl, Sci. Adv. **3**, e1601982 (2017).
[56] K. Morita and T. Tohyama, Phys. Rev. B **99**, 144417 (2019).